Potential COVID-19 papain-like protease PL^{pro} inhibitors: Repurposing FDA-approved drugs using a supercomputer

Valentina L Kouznetsova [1] , **Aidan Zhang** [2] , **Mahidhar Tatineni** [1] , **Mark A Miller** [1] , **Igor F Tsigelny** Corresp. [1, 3, 4]

[1] San Diego Supercomputer Center, University of California, San Diego, La Jolla, California, United States

[2] REHS Program at San Diego Dupercomputer Center, University of California, San Diego, La Jolla, California, United States

[3] Department of Neurosciences, University of California, San Diego, La Jolla, California, United States

[4] Science, CureMatch Inc, San Diego, California, United States

Corresponding Author: Igor F Tsigelny
Email address: itsigeln@ucsd.edu

Using the crystal structure of SARS-CoV-2 papain-like protease (PL^{pro}) as a template, we developed a pharmacophore model of functional centers of the PL^{pro} inhibitor-binding pocket. With this model, we conducted data mining of the conformational database of FDA-approved drugs. This search identified 147 compounds that can be potential inhibitors of SARS-CoV-2 PL^{pro}. The conformations of these compounds underwent 3D fingerprint similarity clusterization, followed by docking of possible conformers to the binding pocket of PL^{pro}. Docking of random compounds to the binding pocket of protease was also done for comparison. Free energies of the docking interaction for the selected compounds were lower than for random compounds. The drug list obtained includes inhibitors of HIV, Hepatitis C, and cytomegalovirus (CMV), as well as a set of drugs that have demonstrated some activity in MERS, SARS-CoV, and SARS-CoV-2 therapy. We recommend testing of the selected compounds for treatment of COVID-19

Potential COVID-19 papain-like protease PL[pro] inhibitors: Repurposing FDA-approved drugs

Valentina L. Kouznetsova[1], Aidan Zhang[2], Mahidhar Tatineni[1], Mark A. Miller[1], Igor F. Tsigelny[1,3,4*]

[1]San Diego Supercomputer Center, UC San Diego, Calif.

[2]REHS program, San Diego Supercomputer Center, UC San Diego, Calif.

[3]Curematch Inc., San Diego, Calif.

[4]Dept. of Neurosciences, UC San Diego, Calif.

*Correspondence to: itsigeln@ucsd.edu

Short Title: COVID-19 papain-like protease inhibitors: Repurposing FDA drugs.

ABSTRACT

Using the crystal structure of SARS-CoV-2 papain-like protease (PL[pro]) as a template, we developed a pharmacophore model of functional centers of the PL[pro] inhibitor-binding pocket. With this model, we conducted data mining of the conformational database of FDA-approved drugs. This search identified 147 compounds that can be potential inhibitors of SARS-CoV-2 PL[pro]. The conformations of these compounds underwent 3D fingerprint similarity clusterization, followed by docking of possible conformers to the binding pocket of PL[pro]. Docking of random compounds to the binding pocket of protease was also done for comparison. Free energies of the docking interaction for the selected compounds were lower than for random compounds. The drug list obtained includes inhibitors of HIV, Hepatitis C, and cytomegalovirus (CMV), as well as a set of drugs that have demonstrated some activity in MERS, SARS-CoV, and SARS-CoV-2 therapy. We recommend testing of the selected compounds for treatment of COVID-19.

30   **One Sentence Summary:** Using pharmacophore-based data mining and computational docking,

31   we selected 147 potential COVID-19 papain-like protease inhibitors.

Introduction

33   Coronaviruses have caused the outbreak of several deadly respiratory diseases since the

34   turn of the 21st century, such as the severe acute respiratory syndrome (SARS) in 2002 and the

35   Middle East respiratory syndrome (MERS) in 2012, in addition to the recent COVID-19 pandemic,

36   which has claimed more than 489 000 lives with over 9.5 million confirmed cases worldwide.

37   Despite the profound impact of these viral outbreaks on public health and the economy, effective

38   vaccines have not been found for either SARS or MERS viruses. In view of the ongoing pandemic,

39   and the absence of vaccines, there is an immediate need to find drugs to treat patients.

40   Viral proteases are an attractive target for drug development. Viral proteases are essential for

41   replication, and are unique to each virus, thus offering the potential for highly specific treatments

42   that produce minimal toxic side effects. Viral protease Inhibitors such as indinavir targeting a

43   single protease in HIV-1, ritonavir targeting the single proteases in HIV-1 and HIV-2, and

44   boceprevir targeting NS3 protease of HCV have been used to effectively treat a variety of viral

45   infections [1]. For coronaviruses, host protease TMPRSS2 provide a possible target where

46   protease inhibitors can prevent viral entry [2-4]. On the other hand, two viral proteases, PL^{pro}

47   (papain-like protease) and 3CL^{pro} (chymotrypsin-like protease, aka main protease) are also

48   attractive as druggable targets [5,6]. Both proteases are highly conserved specific nsps: nsp5 for

49   3CL^{pro} and nsp3 for PL^{pro}. Nsp3 is a large (200 000 kDa) multi-domain polypeptide that provides

50   the membrane anchored scaffolding structure required for the replication/transcription complex

51   (RTC) of coronaviruses [7]. In addition to PL^{pro}, the C-terminus of nsp3 contains transmembrane

52   domains that anchor the protein and a dsDNA, unwinding/RNA binding domain that is essential

53   for replicase activity [8]. Residing within the 213-kDa, membrane-associated replicase product

54   nsp3, the SARS-CoV PL^{pro} is responsible for cleaving junctions spanning nsp1 to nsp4 [9].

55   Studies of Harcourt and colleagues [10] revealed that PL^{pro} can cleave at the three predicted

56   cleavage sites and that it requires membrane association to process the nsp3/4 cleavage site.

57   It is a particularly attractive drug target because it plays an essential role in processing the

58   viral polyproteins to create the mature nsp3, as well as helping the coronavirus evade host immune

59   response via competitive interaction with ubiquitin and ISG15 on host-cell proteins [7,11-13].

60   Although no protease inhibitors are currently available for treatment of SARS, MERS, or COVID-

61   19, studies of inhibitors of the MERS, SARS-CoV, and SARS-CoV-2 PL^{pro} are underway and

62   reports have appeared that such protease inhibitors can prevent SARS-CoV replication in cultured

63   cells [12,14-16].

64   In view of the urgent need for effective treatments and the high cost of developing new

65   drugs (both in terms of time and resources), repurposing FDA-approved drugs is an efficient

66   strategy for identifying drug candidates that can be used immediately in the COVID-19 pandemic

67   [17, 19]. In a previous report, we [19] and others [20-24] have used molecular modeling studies to

68   identify FDA-approved drugs and other compounds [21,22,24,25] that are predicted to bind to

69   3CL^{pro}. The list of potential inhibitors includes bleomycin, mithramycin, and goserelin, as well as

70   others that may be effective [19]. Here we report a similar screen of FDA-approved drugs for

71   potential inhibitors of SARS-COV-2 PL^{pro} using the recently reported structure of SARS-CoV-2

72   PL^{pro} (PDB ID: 6W9C) [26,27].

73   **Methods**

74   *Pharmacophore design and use*

75   Analyzing a pocket, we elucidated a majority of possible interactions between PL^{pro} (PDB ID:

76   6W9C) and a potential ligand for developing a protein-based pharmacophore model with potential

77   fictional centers that would bind to the residues in the pocket (Figure 1A). Resolution of the protein

78   structure used in the study is 2.7A. From our experience such a resolution is not the best but

79   sufficient for the pharmacophore-based modeling. Using Molecular Operating Environment

80   (MOE; CCG, Montreal, Canada), we constructed two pharmacophore models including ten

81   features (Pha01) and ten features with excluded volume R=1.3 Å (Pha02): two donors, two donors

82   or acceptors, one hydrophobic, and five hydrophobic or aromatic features (Figure 1A). Based on

83   developed pharmacophores to select potential drug-candidates, we conducted a pharmacophore

84   search with both pharmacophore models on our conformational database (DB) of FDA-approved

85   drugs, containing around 2500 drugs and 600 000 conformations. Searches were provided using

86   pharmacophores partial match: eight of ten features for Pha01 and seven of ten features for Pha02.

87   Search results of Pha01 (Search 1) identified 405 compounds with 63 821 conformations while

88   Pha02 (Search 2) identified 857 compounds with 224 609 conformations. We selected 84 and 77

89   compounds from Search 1 and 2 respectively based on a number of H-bonds and hydrophobic

90   interactions in the best docking pose. Because some compounds appeared in both searches, we

91   eliminated duplicate compounds, resulting in a total of 147 unique drugs. Then we clustered the

92   selected 147 compounds, using MOE Database Viewer with a fingerprint GpiDAPH3 and

93   similarity–overlap parameter $SO = 42\%$ to elucidate the common structure-functional features of

94   the groups of compound to enhance further drug development.

95   ***Docking of drug conformers using the supercomputer Comet***

96   For docking the selected compounds, we used the crystal structure of the SARS-CoV-2 PLP (PDB

97   ID: 6W9C). A binding pocket was defined based on the known residues of the S3/S4 binding

98   pocket site of SARS-CoV-2 PLP. Docking of the selected compounds was done using Autodock

99   Vina. Conformers of each of the selected compounds were generated using OpenBabel. However,

100   since Autodock Vina does not support docking compounds that include boron atoms (i.e.,

101   bortezomib), each boron atom in the conformers of bortezomib was replaced with carbon atoms

102   due to their similar size. The random control compounds were selected by a 79-compound, simple-

103   random subset of all the ZINC DB compounds; these were docked with PL^{pro} in the same

104   processes. Likewise, the conformers of the compound with ID: ZINC001779539170 had their

105   silicon atom replaced with carbon due to Autodock Vina's restraints regarding supported atoms.

106   The Comet supercomputer at the San Diego Supercomputer Center (SDSC) was primarily used

107   for two parts of the analyses: (1) conversion of files in the pdb format to the pdbqt format, using

108   the Open Babel software (version 2.4.1), and (2) all the docking computations using the AutoDock

109   Vina software (version 1.1.2). We outline the system configuration and the analyses workflow

110   details below.

111   *The Comet supercomputing system*

112   Comet is an NSF funded cluster (NSF grant: ACI #1341698) designed by Dell and SDSC

113   delivering 2.76 peak petaflops. It features Intel Haswell processors with AVX2, Mellanox FDR

114   InfiniBand interconnects, and Aeon storage [28]. There are 1944 standard compute nodes and 72

115   GPU nodes. The standard compute nodes consist of Intel Xeon E5-2680v3 (Haswell) processors,

116   128 GB DDR4 DRAM (64 GB per socket), and 320 GB of SSD local scratch memory. The GPU

117   nodes contain four NVIDIA GPUs each. There are four large memory nodes containing 1.5 TB of

118   DRAM and four Haswell processors each. All the computations for this paper were conducted on

119   the standard compute nodes and made extensive use of the local scratch filesystems.

120   *File conversion and docking workflow*

121   The first step in the computational workflow on Comet was to convert 385 193 pdb files of drug

122   conformers into the pdbqt format. The files were contained in 27 zip files and the jobs were

123   simultaneously run on Comet (one zip file in each job). The zip files were extracted to the local

124   SSD based file system to reduce IO loads, converted to pdbqt files in the same location, and then

125   the results were archived in a zip file. With the local SSD approach, all the conversion jobs were

126   completed in less than 20 minutes.

127   The AutoDock Vina software was used to dock a total of 490 678 drug conformers using

128   computations on Comet. The local SSD approach was used again to mitigate IO loads on the

129   main filesystem. The docking tasks were split up into separate jobs (that were run

130   simultaneously) with 3000–4000 drug conformers docked in each job. All the individual docking

131   computations were conducted using 8 cores (The parallelism is limited by the exhaustiveness

132   parameter, set to 8 for the analysis) and scaling tests showed an excellent parallel efficiency of

133   93.2%. New 16. Coronavirus disease (COVID-19) Situation Report–171, WHO 9 July2020

134   https://www.who.int/docs/default-source/coronaviruse/situation-reports/20200709-covid-19-sitrep-

135   171.pdf?sfvrsn=9aba7ec7_2)

136

137

Results

139   Among the compounds selected by the pharmacophore search of FDA-approved drug DB, we

140   identified two clusters (A and B) containing twenty compounds; three clusters (C, D, and E)

141   containing nine, five, and ten compounds correspondingly; two clusters (F and G) with four, and

142   three clusters (H, I, and J) with three compounds; along with ten two-compounds clusters and 46

143   not clustered single compounds. Compounds in clusters A–G are listed in Table 1, other

144   compounds can be found in Supplemental Materials (Table S1). Flexible alignment of clusters B

145   and C were used to illustrate compounds' common features (Figure 2).

146   **Figure 1.** Insert here

147   Interesting to note that this selection contained the best docking energy drug nilotinib that
148   showed activity against SARS-CoV.

149   **Table 1.** Insert here

150

151   Figure 2A and B shows the flexible alignments of clusters B and C containing the drugs with the
152   best docking energies.

153

154

155   **Figure 2.** Insert here

156   To define the putative best binding drugs, we conducted docking of multiple conformers of drugs
157   selected from a pharmacophore-based search and of random compounds to the binding site of
158   COVID-19 papain-like protease. The random control compounds were selected by a 79-
159   compound, simple-random subset of the ZINC DB of drug-like compounds. For docking the
160   selected compounds, we used the same crystal structure of the SARS-CoV-2 (Protein Data Bank
161   entry, 6W9C) imported into MOE. A S3/S4 pocket site was defined, which included the following
162   residues: K157, L162, G163, D164, R166, P247, P248, Y264, G266, Y268, and P299. Conformers
163   of each of the selected compounds were generated with OpenBabel before being docked with
164   AutoDock Vina.

165   Figure 3 shows the values of docking free energies of the selected and random compounds.
166   The energies of interaction with PL^{pro} are shown in Table 2. One can see that drugs of clusters 2
167   and 5 are at the top of the table. Note that the binding pocket of PL^{pro} is not very specific and
168   contains a number of hydrophobic binding centers; that is why binding energies are not
169   overwhelmingly better than those of random compounds (Figure 3). At the same time, we want
170   also note that the values of energies in the table can be used with discretion. Binding positions of
171   ligands in the pockets of proteins in many cases do not have minimal energies.

172

173   **Figure 3.** Inset here

174

175   **Table 2.** Insert here

176
177   **Figure 4**. Insert here

Discussion

179
180   Based on the crystal structure of SARS-CoV-2 PL^{pro} (PDB ID: 6W9C), we developed two

181   pharmacophore models of the binding pocket of this protein. Using these models, we browsed our

182   conformational database of FDA-approved drugs and obtained 147 hits that were clusterized for

183   selecting the most promising candidates and then used for multi-conformational docking to the

184   PL^{pro} pocket. The drug list obtained includes inhibitors of HIV, Hepatitis C, and CMV, as well as

185   a set of drugs that demonstrated some activity in MERS, SARS-CoV, and SARS-CoV-2 therapy.

186   We developed a pharmacophore model of the binding pocket site S3/S4 of COVID-19 PL^{pro} then

187   conducted multi-conformational docking of these drug compounds to this site for ranging the

188   potential inhibitors selected by pharmacophore-based search. We also conducted clusterization of

189   the selected compounds based on their pharmacophores 3D profiles to elucidate the common

190   features for further drug design, and compared the docking results for the selected drug compounds

191   with the docking results of random compounds to evaluate the area of significance in the values

192   of binding energies. We note that the pharmacophore-based selection is a very powerful tool so

193   even the drugs with the binding energies on the same level with the random compound do not have

194   to be completely discarded.

195   We are aware of two other studies where docking experiments were used to predict binding of

196   existing pharmaceuticals to the SARS-CoV-2 PL^{pro} [9,18]. Both prior studies relied on homology

197   modelling of part [21] or the entire SARS-CoV PL^{pro}. Wu et al [21] studied 2924 compounds from

198   ZINC Drug Database, as well as 78 known antivirals; while Arya et al. studied 2525 FDA-

199   approved compounds from DrugBank and the ZINC 15 database. Two compounds were identified

200   in the present study and by Wu et al [9]: valganciclovir and pemextred. The remaining compounds

201   identified here are unique to our study. This may reflect the influence of using the crystal structure

202   of SARS-CoV-2 as the starting point in the present study, and a difference in methodology in our

203   case including preliminary pharmacophore-based search before docking computational

204   experiments.

205   It is interesting to note that several drugs with high docking energy were tested or are in

206   experimental testing: nilotinib was active only for SARS-CoV [26]; dasatinib was confirmed to be

207   active in cell-culture assays for MERS-CoV and SARS-CoV [27]. Dasatinib was also shown to be

208   active against SARS-Cov-2 in clinical cases [30]. Terconazole and fluspirilene were shown to be

209   active in cell-culture assays for SARS-Cov-2 [30]. Manidipine was found in the database of

210   experimental results for broad set of antiviral drugs, DrugVirus.info [31]. Indinavir and ritonavir

211   (HIV viral protease inhibitor), boceprevir (Hepatitis C protease inhibitor), and valganciclovir

212   (antiviral medication for CMV) were found with energies of binding to PL^{pro} of -6.7 kcal/mol and

213   better. We note that according to the DrugVirus.info database [31], 11 of the compounds selected

214   by the pharmacophore-based search showed activity against the set of viruses (Fig. 4) including

215   amodiaquine, chloroquine, sorafenib, dasatenib, hydroxychloroquine, bortezomib, topotecan,

216   manidipine, lovastatin, gefitinib, and ritonavir. Most experimental testing was done in cell-

217   cultures, but there is also a significant amount of animal testing and several of these drugs are in

218   different stages of clinical trials. The prior computational studies [10,21] did not identify any of

219   these compounds as potential inhibitors of PL^{pro}, with the exception of chloroquine [21]. On the

220   other hand, Wu et al. [10] identified two antivirals that our experiments did not predict as

221   inhibitors: ribavirin and β-thymidine.

Acknowledgements

223   We would like to thank the people of San Diego Supercomputer Center and CureMatch, Inc., for
224   friendly support.

225   **Funding:** The SDSC Comet supercomputer is supported by the NSF grant: ACI #1341698
226   Gateways to Discovery: Cyberinfrastructure for the Long Tail of Science. MAM was supported
227   by NIH R01 GM126463.

228   **Author contributions:** IFT and VLK introduced initial idea of the project; VLK conducted
229   pharmacophore development, databases searches, and clustering and multiconfromational
230   alignment; MAM, IFT, and VLK conducted interpretation of the results AZ and MT conducted
231   computational docking on Comet supercomputer; IFT, VLK, MAM, and AZ wrote the article.

232   **Competing interests:** Authors declare no competing interests.

233

References

235   1.   Anderson, J., Schiffer, C., Lee, S.-K., and Swanstrom, R. (2009) Viral Protease Inhibitors. in
236   *Antiviral Strategies* (Kräusslich, H.-G., and Bartenschlager, R. eds.), Springer Berlin Heidelberg,
237   Berlin, Heidelberg. pp 85–110. 10.1007/978-3-540-79086-0_4

238   2.   Hoffmann, M., Kleine-Weber, H., Schroeder, S., Krüger, N., Herrler, T., Erichsen, S., Schiergens,
239   T. S., Herrler, G., Wu, N. H., Nitsche, A., Müller, M. A., Drosten, C., and Pöhlmann, S. (2020)
240   SARS-CoV-2 Cell Entry Depends on ACE2 and TMPRSS2 and Is Blocked by a Clinically
241   Proven Protease Inhibitor. *Cell* **181**, 271–280.e278. 10.1016/j.cell.2020.02.052

242   3.   Simmons, G., Gosalia, D. N., Rennekamp, A. J., Reeves, J. D., Diamond, S. L., and Bates, P.
243   (2005) Inhibitors of cathepsin L prevent severe acute respiratory syndrome coronavirus entry.
244   *Proc Natl Acad Sci U S A* **102**, 11876–11881. 10.1073/pnas.0505577102

245   4.   Zhou, Y., Vedantham, P., Lu, K., Agudelo, J., Carrion, R., Jr., Nunneley, J. W., Barnard, D.,
246   Pöhlmann, S., McKerrow, J. H., Renslo, A. R., and Simmons, G. (2015) Protease inhibitors
247   targeting coronavirus and filovirus entry. *Antiviral research* **116**, 76–84.
248   10.1016/j.antiviral.2015.01.011

249   5.   Vuong, W., Khan, M. B., Fischer, C., Arutyunova, E., Lamer, T., Shields, J., Saffran, H. A.,
250   McKay, R. T., van Belkum, M. J., Joyce, M., Young, H. S., Tyrrell, D. L., Vederas, J. C., and
251   Lemieux, M. J. (2020) Feline coronavirus drug inhibits the main protease of SARS-CoV-2 and
252   blocks virus replication. *bioRxiv*, 2020.2005.2003.073080. 10.1101/2020.05.03.073080

253   6.   Ma, C., Sacco, M. D., Hurst, B., Townsend, J. A., Hu, Y., Szeto, T., Zhang, X., Tarbet, B., Marty,
254   M. T., Chen, Y., and Wang, J. (2020) Boceprevir, GC-376, and calpain inhibitors II, XII inhibit
255   SARS-CoV-2 viral replication by targeting the viral main protease. *bioRxiv*,
256   2020.2004.2020.051581. 10.1101/2020.04.20.051581

257   7.   Lei, J., Kusov, Y., and Hilgenfeld, R. (2018) Nsp3 of coronaviruses: Structures and functions of a
258   large multi-domain protein. *Antiviral Research* **149**, 58–74.
259   https://doi.org/10.1016/j.antiviral.2017.11.001

260   8.   Neuman, B. W. (2016) Bioinformatics and functional analyses of coronavirus nonstructural
261   proteins involved in the formation of replicative organelles. *Antiviral Research* **135**, 97–107.
262   https://doi.org/10.1016/j.antiviral.2016.10.005

263   9.   Devaraj, S. G., Wang, N., Chen, Z., Chen, Z., Tseng, M., Barretto, N., Lin, R., Peters, C. J.,
264   Tseng, C.-T. K., Baker, S. C., and Li, K. (2007) Regulation of IRF-3-dependent Innate Immunity
265   by the Papain-like Protease Domain of the Severe Acute Respiratory Syndrome Coronavirus.
266   *Journal of Biological Chemistry* **282**, 32208-32221. 10.1074/jbc.M704870200

267   10.   Harcourt, B. H., Jukneliene, D., Kanjanahaluethai, A., Bechill, J., Severson, K. M., Smith, C. M.,
268   Rota, P. A., and Baker, S. C. (2004) Identification of Severe Acute Respiratory Syndrome
269   Coronavirus Replicase Products and Characterization of Papain-Like Protease Activity. J Virol
270   78, 13600-13612. 10.1128/jvi.78.24.13600-13612.2004

271   11.   Wu, C., Liu, Y., Yang, Y., Zhang, P., Zhong, W., Wang, Y., Wang, Q., Xu, Y., Li, M., Li, X.,
272   Zheng, M., Chen, L., and Li, H. (2020) Analysis of therapeutic targets for SARS-CoV-2 and
273   discovery of potential drugs by computational methods. *Acta Pharmaceutica Sinica B* **10**, 766–
274   788. https://doi.org/10.1016/j.apsb.2020.02.008

275   12.   Báez-Santos, Y. M., St. John, S. E., and Mesecar, A. D. (2015) The SARS-coronavirus papain-
276   like protease: Structure, function and inhibition by designed antiviral compounds. *Antiviral*
277   *Research* **115**, 21–38. https://doi.org/10.1016/j.antiviral.2014.12.015

278   13.   Lei, J., Mesters, J. R., Drosten, C., Anemüller, S., Ma, Q., and Hilgenfeld, R. (2014) Crystal
279   structure of the papain-like protease of MERS coronavirus reveals unusual, potentially druggable
280   active-site features. *Antiviral Research* **109**, 72–82.
281   https://doi.org/10.1016/j.antiviral.2014.06.011

282   14.   Ratia, K., Pegan, S., Takayama, J., Sleeman, K., Coughlin, M., Baliji, S., Chaudhuri, R., Fu, W.,
283   Prabhakar, B. S., Johnson, M. E., Baker, S. C., Ghosh, A. K., and Mesecar, A. D. (2008) A
284   noncovalent class of papain-like protease/deubiquitinase inhibitors blocks SARS virus
285   replication. *Proceedings of the National Academy of Sciences* **105**, 16119–16124.
286   10.1073/pnas.0805240105

287   15.   Lee, H., Lei, H., Santarsiero, B. D., Gatuz, J. L., Cao, S., Rice, A. J., Patel, K., Szypulinski, M.
288   Z., Ojeda, I., Ghosh, A. K., and Johnson, M. E. (2015) Inhibitor recognition specificity of MERS-
289   CoV papain-like protease may differ from that of SARS-CoV. *ACS Chem Biol* **10**, 1456–1465.
290   10.1021/cb500917m

291   16.   Akaji, K., Konno, H., Mitsui, H., Teruya, K., Shimamoto, Y., Hattori, Y., Ozaki, T., Kusunoki,
292   M., and Sanjoh, A. (2011) Structure-Based Design, Synthesis, and Evaluation of Peptide-Mimetic
293   SARS 3CL Protease Inhibitors. *Journal of Medicinal Chemistry* **54**, 7962–7973.
294   10.1021/jm200870n

295   17.   Tan, E., L. C. , Ooi, E. E., Lin, C.-Y., Tan, H. C., Ling, A. E., Lim, B., and Stanton, L., W. (2004)
296   Inhibition of SARS Coronavirus Infection In Vitro with Clinically Approved Antiviral Drugs.
297   *Emerging Infectious Disease journal* **10**, 581. 10.3201/eid1004.030458

298   18.   Coronavirus disease (COVID-19) Situation Report–171, WHO 9 July2020
299   https://www.who.int/docs/default-source/coronaviruse/situation-reports/20200709-covid-19-
300   sitrep-171.pdf?sfvrsn=9aba7ec7_2)

301   19.   Kouznetsova, V., Huang, D., and Tsigelny, I. F. (2020) Potential COVID-19 Protease Inhibitors:
302   Repurposing FDA approved Drugs. *ChemRxiv* 10.26434/chemrxiv.12093900.v1

303   20.   Kandeel, M., and Al-Nazawi, M. (2020) Virtual screening and repurposing of FDA approved
304   drugs against COVID-19 main protease. *Life Sciences* **251**, 117627.
305   https://doi.org/10.1016/j.lfs.2020.117627

306   21.   Arya, R., Das, A., Prashar, V., and Kumar, M. (2020) *Potential Inhibitors Against Papain-like*
307   *Protease of Novel Coronavirus (COVID-19) from FDA Approved Drugs*,
308   10.26434/chemrxiv.11860011

309   22.   Liu, X., and Wang, X.-J. (2020) Potential inhibitors for 2019-nCoV coronavirus M protease from
310   clinically approved medicines. *bioRxiv*, 2020.2001.2029.924100. 10.1101/2020.01.29.924100

311   23.   Plewczynski, D., Hoffmann, M., Von Grotthuss, M., Ginalski, K., and Rychewski, L. (2007) In
312   Silico Prediction of SARS Protease Inhibitors by Virtual High Throughput Screening. *Chemical*
313   *Biology & Drug Design* **69**, 269–279. 10.1111/j.1747-0285.2007.00475.x

314   24.   Ton, A.-T., Gentile, F., Hsing, M., Ban, F., and Cherkasov, A. (2020) Rapid Identification of
315   Potential Inhibitors of SARS-CoV-2 Main Protease by Deep Docking of 1.3 Billion Compounds.
316   *Molecular Informatics* **n/a** 10.1002/minf.202000028

317 25.   Alamri, M. A., Tahir ul Qamar, M., and Alqahtani, S. M. (2020) Pharmacoinformatics and
318   Molecular Dynamic Simulation Studies Reveal Potential Inhibitors of SARS-CoV-2 Main
319   Protease 3CLpro. *Preprints 2020, 2020020308* 10.20944/preprints202002.0308.v1

320 26.   Zhang, L., Lin, D., Sun, X., Curth, U., Drosten, C., Sauerhering, L., Becker, S., Rox, K., and
321   Hilgenfeld, R. (2020) Crystal structure of SARS-CoV-2 main protease provides a basis for design
322   of improved α-ketoamide inhibitors. *Science* **368**, 409–412. 10.1126/science.abb3405

323 27.   Osipiuk, J., Jedrzejczak, R., Tesar, C., Endres, M., Stols, L., Babnigg, G., Kim, Y., Michalska,
324   K., and Joachimiak, A. (2020) The crystal structure of papain-like protease of SARS CoV-2,
325   2020. 10.2210/pdb6W9C/pdb

326 28.   Richard L. Moore, Chaitan Baru, Diane Baxter, Geoffrey C. Fox, Amit Majumdar, Phillip
327   Papadopoulos, Wayne Pfeiffer, Robert S. Sinkovits, Shawn Strande, Mahidhar Tatineni, Richard
328   P. Wagner, Nancy Wilkins-Diehr, and Michael L. Norman. 2014. Gateways to Discovery:
329   Cyberinfrastructure for the Long Tail of Science. In Proceedings of the 2014 Annual Conference
330   on Extreme Science and Engineering Discovery Environment (XSEDE '14). Association for
331   Computing Machinery, New York, NY, USA, Article 39, 1–8.
332   DOI:https://doi.org/10.1145/2616498.2616540

333 29   Dyall J, Coleman CM, Hart BJ, et al. (2014). Repurposing of clinically developed drugs for
334   treatment of Middle East respiratory syndrome coronavirus infection. *Antimicrobial Agents and*
335   *Chemotherapy* 58, 8, 4885–4893

336 30   Abruzzese E., Luciano L., D'Agostino F., Trawinska M. M., Pane F., De Fabritiis P. SARS-CoV-
337   2 (COVID-19) and Chronic Myeloid Leukemia (CML): a case report and review of ABL kinase
338   involvement in infection. *Mediterr J Hematol Infect Dis* 2020, 12(1): e2020031, DOI:
339   http://dx.doi.org/10.4084/MJHID.2020.031

340 31   Andersen PI, Ianevski A, Lysvand H, Vitkauskiene A, et al. Discovery and Development of Safe-
341   In-Man Broad-Spectrum Antiviral Agents. *Int J Infect Dis*. 2020 Apr;93:268–276. doi:
342   10.1016/j.ijid.2020.02.018.

343

344 **Figure Legends.**

345 **Figure 1.** Binding position of the drugs with the best scores in papain-like protease. **(A)** Ten
346 features pharmacophore. The model contains ten functional centers: two donors, two donors or
347 acceptor centers, one hydrophobic center, and five hydrophobic or aromatic centers (excluded
348 volume is hidden). **(B)** Dihydroergocryptine, docking free energy (DFE) = −8.0 kcal/mol. **(C)**
349 Enasidenib, (DFE) = −8.1 kcal/mol. **(D)** Irinotecan, (DFE) = −8.5 kcal/mol. **(E)** Levomefolic acid,
350 (DFE) = −8.4 kcal/mol. **(F)** Nilotinib, (DFE) = −9.3 kcal/mol. **(G)** Siponimod, (DFE) = −8.0
351 kcal/mol. **(H)** Sorafenib, (DFE) = −8.0 kcal/mol.

352 **Figure 2.** Flexible alignments of compounds in clusters selected by the pharmacophore-based
353 search of possible drug-candidates in the conformational database of FDA-approved drugs having
354 the best docking energies. **(A)** Cluster B (20 compounds), **(B)** Cluster C (9 compounds).

355 **Figure 3.** Free energies of docking interactions of selected and random compounds with PL^{pro}.
356 Minimal energies of the selected and random compounds are -9.3 and -7.7 kcal/mol respectively.

357 **Figure 4**. Drugs among the predicted by pharmacophore search inhibitors of PL^{pro} that were
358 experimentally tested for various viruses (Obtained using DrugVirus.info database [26]).

359

Figure 1

Ten features pharmacophore of papin-like protease binding pocket..

The model contains ten functional centers: two donors, two donors or acceptor centers, one hydrophobic center, and five hydrophobic or aromatic centers (excluded volume is hidden).
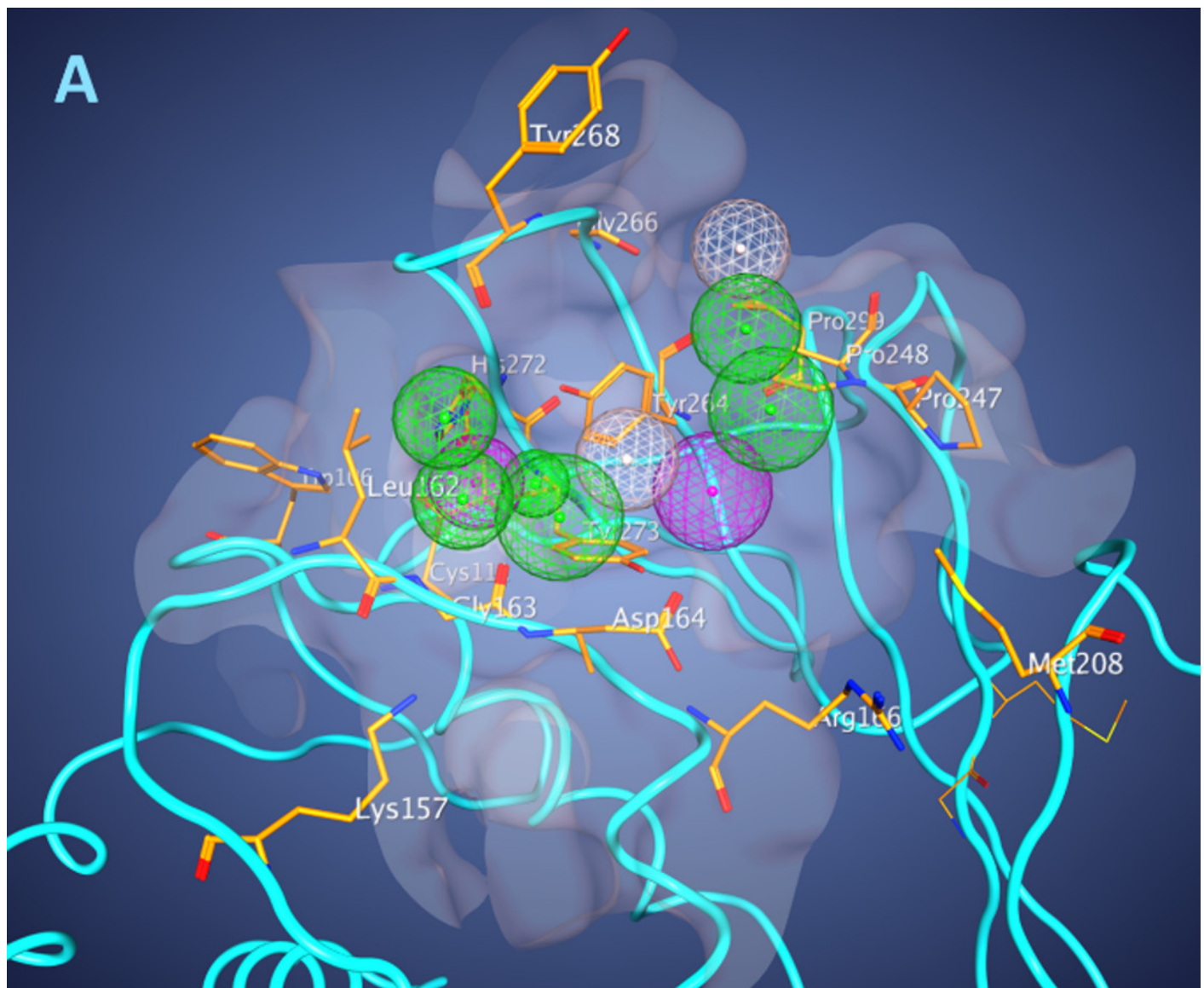
Figure 2

Binding position of the drugs with the best scores in papain-like protease.

Dihydroergocryptine, docking free energy (DFE) = −8.0 kcal/mol.
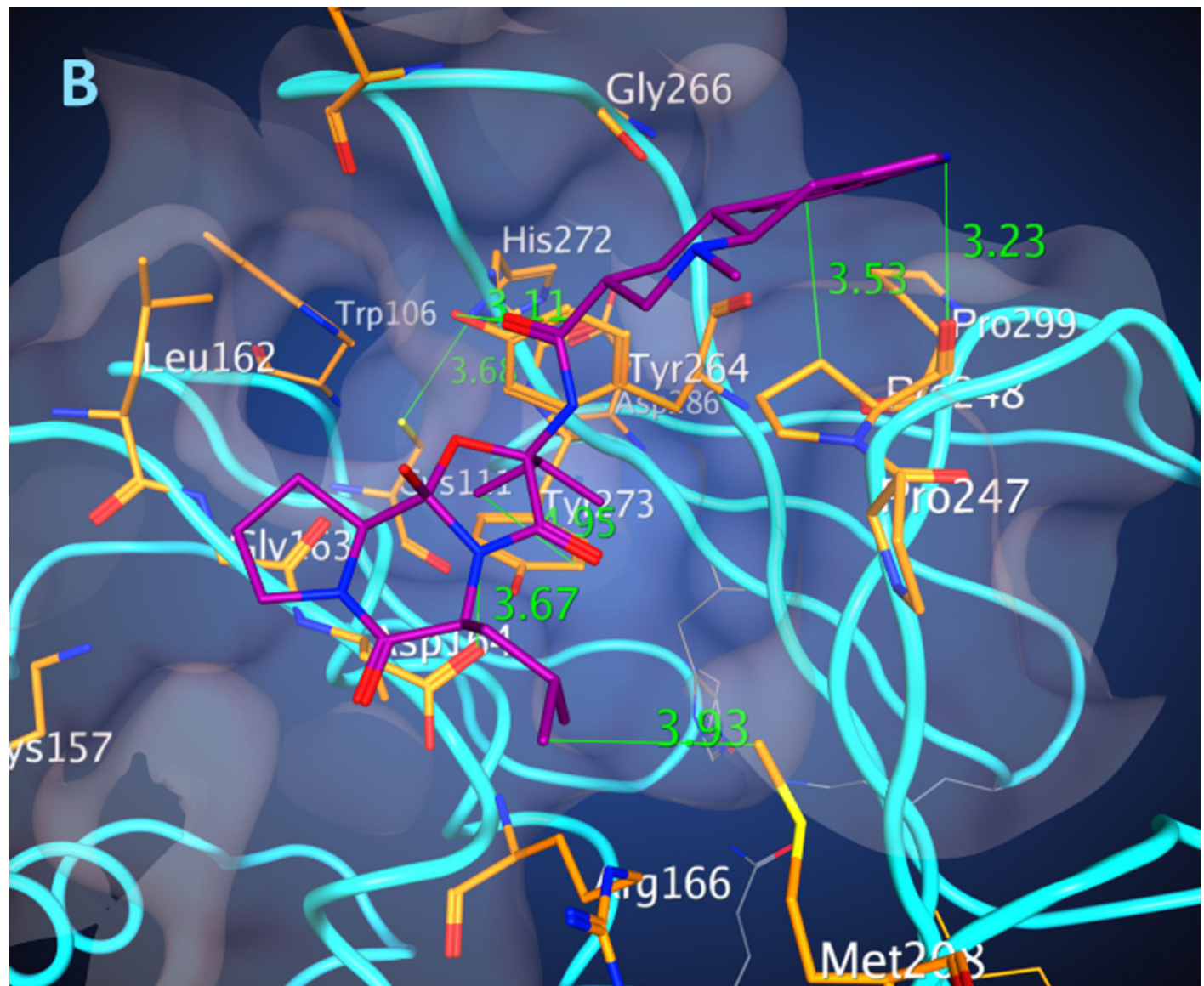
Figure 3

Binding position of the drugs with the best scores in papain-like protease.

Enasidenib, (DFE) = −8.1 kcal/mol.
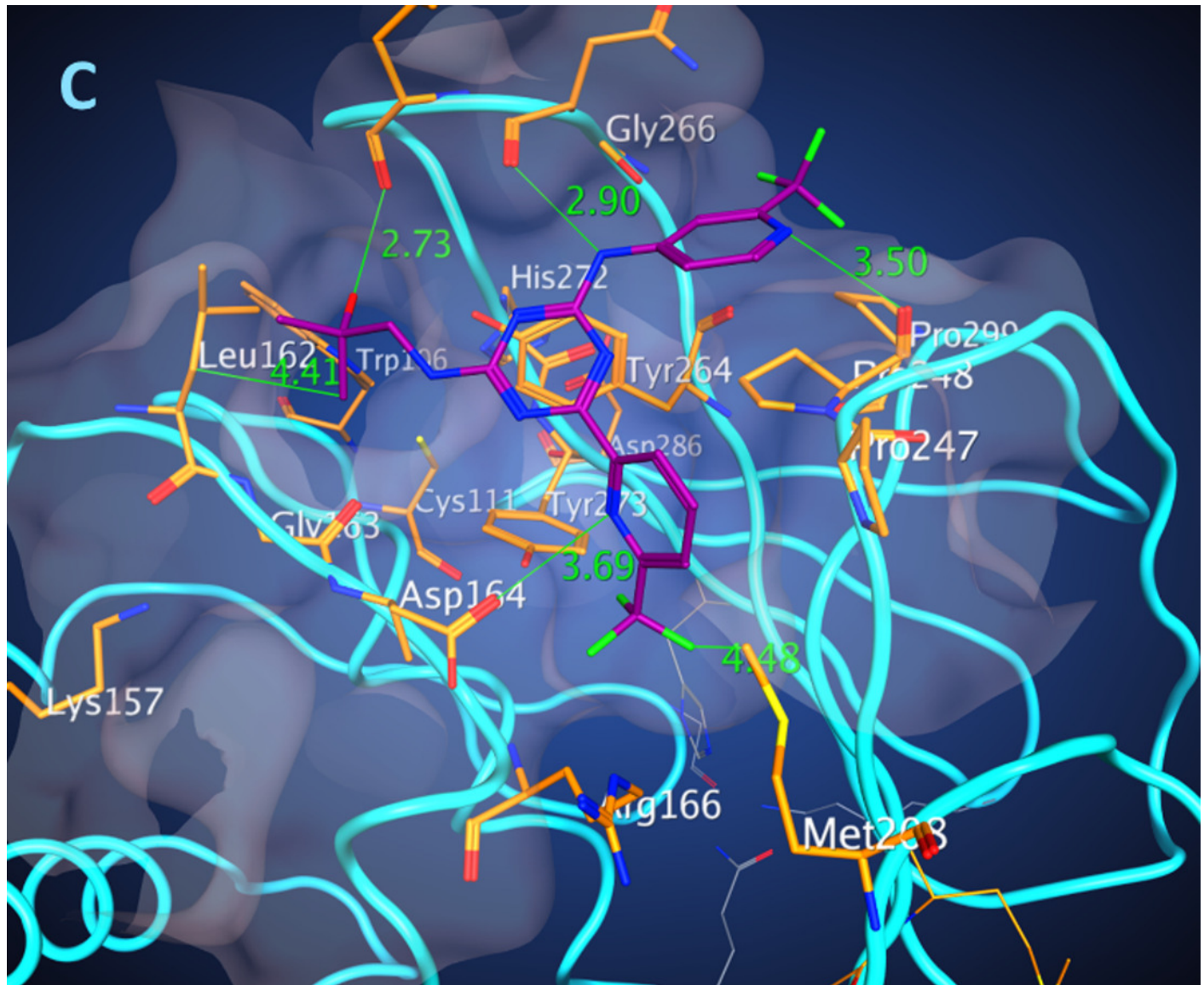
Figure 4

Binding position of the drugs with the best scores in papain-like protease.

Irinotecan, (DFE) = −8.5 kcal/mol.

Figure 5

Binding position of the drugs with the best scores in papain-like protease. (A) Ten features pharmacophore.

Levomefolic acid, (DFE) = −8.4 kcal/mol.
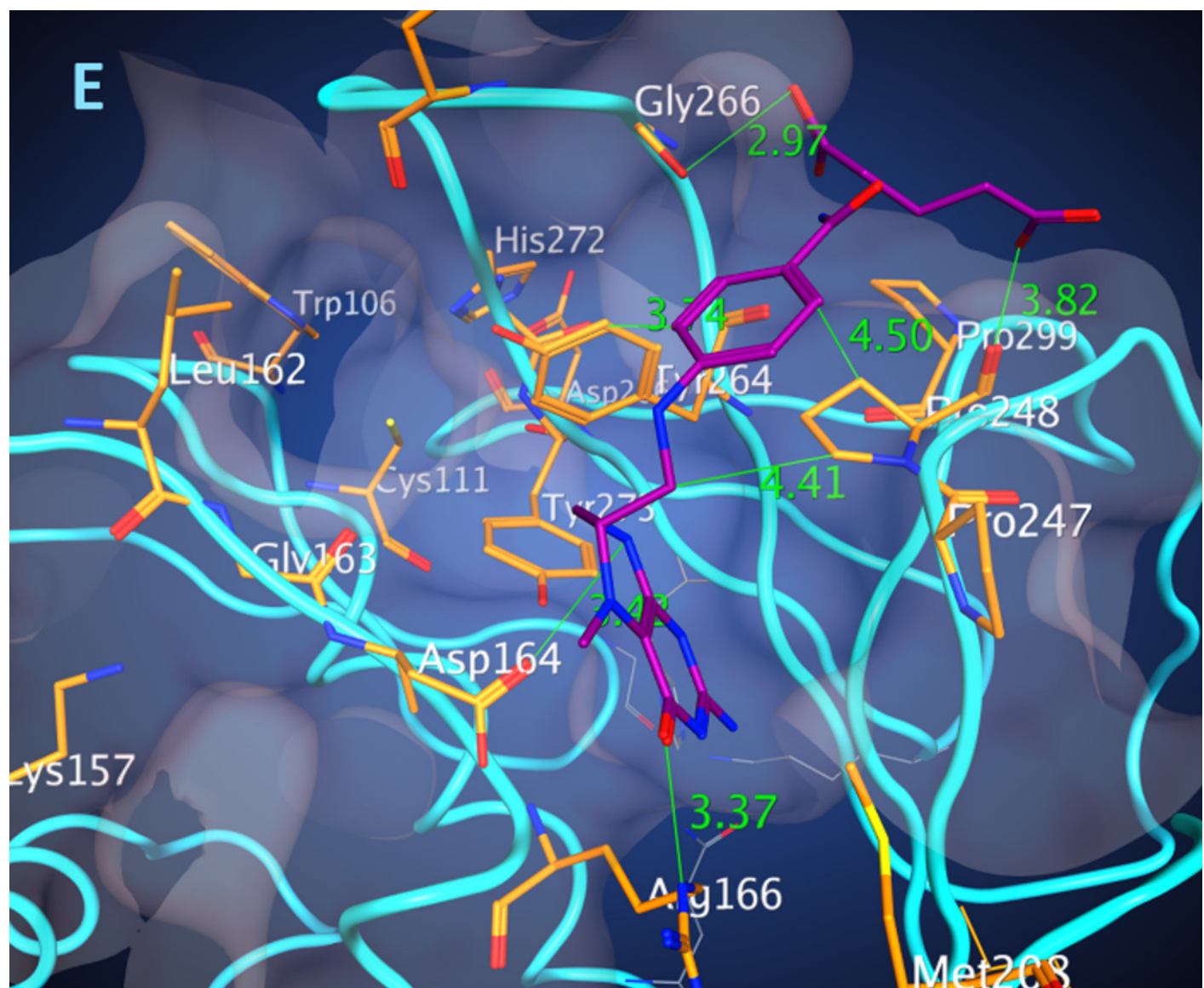
Figure 6

Binding position of the drugs with the best scores in papain-like protease. (A) Ten features pharmacophore.

Nilotinib, (DFE) = −9.3 kcal/mol.
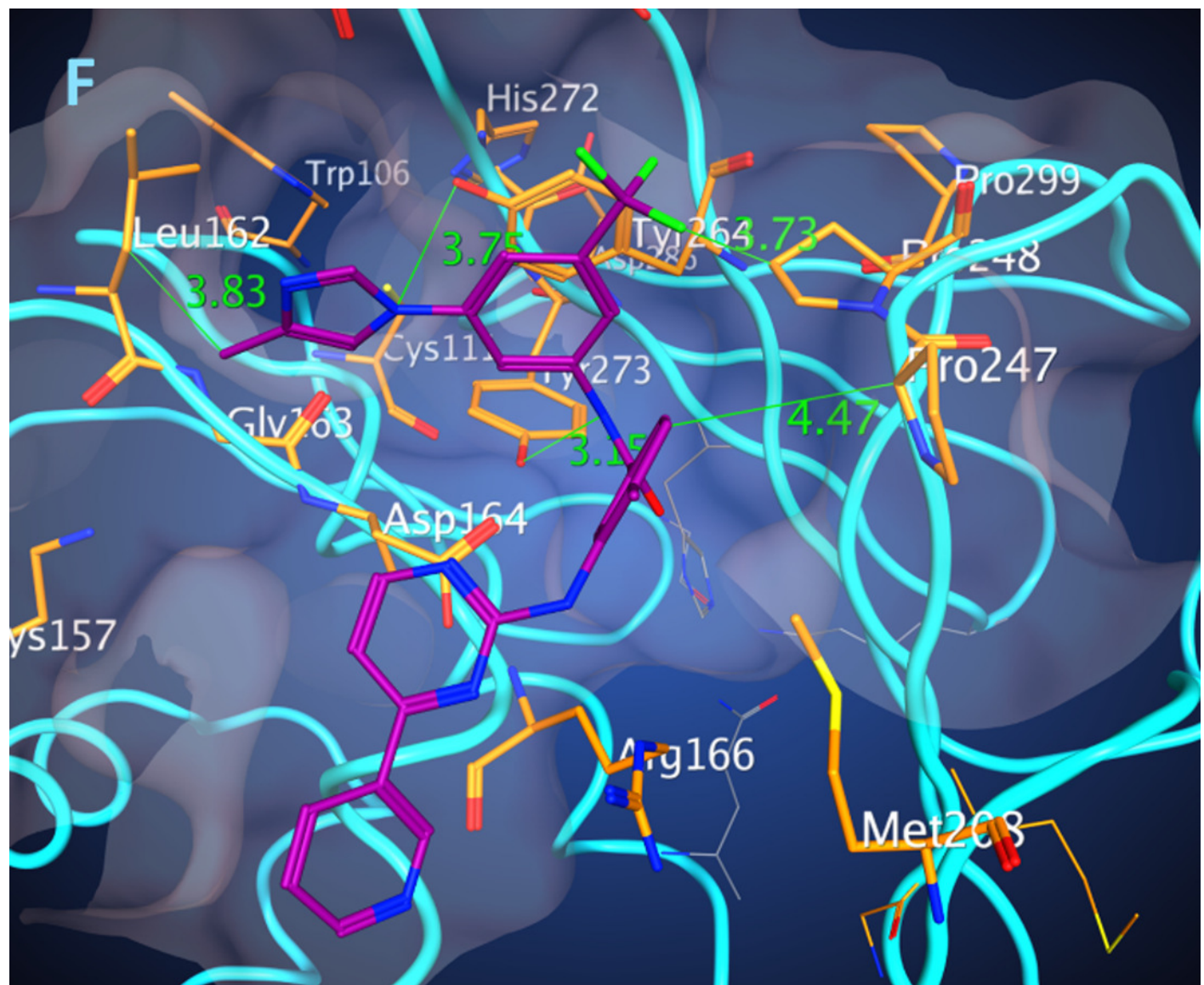
Figure 7

Binding position of the drugs with the best scores in papain-like protease. (A) Ten features pharmacophore.

Siponimod, (DFE) = −8.0 kcal/mol.
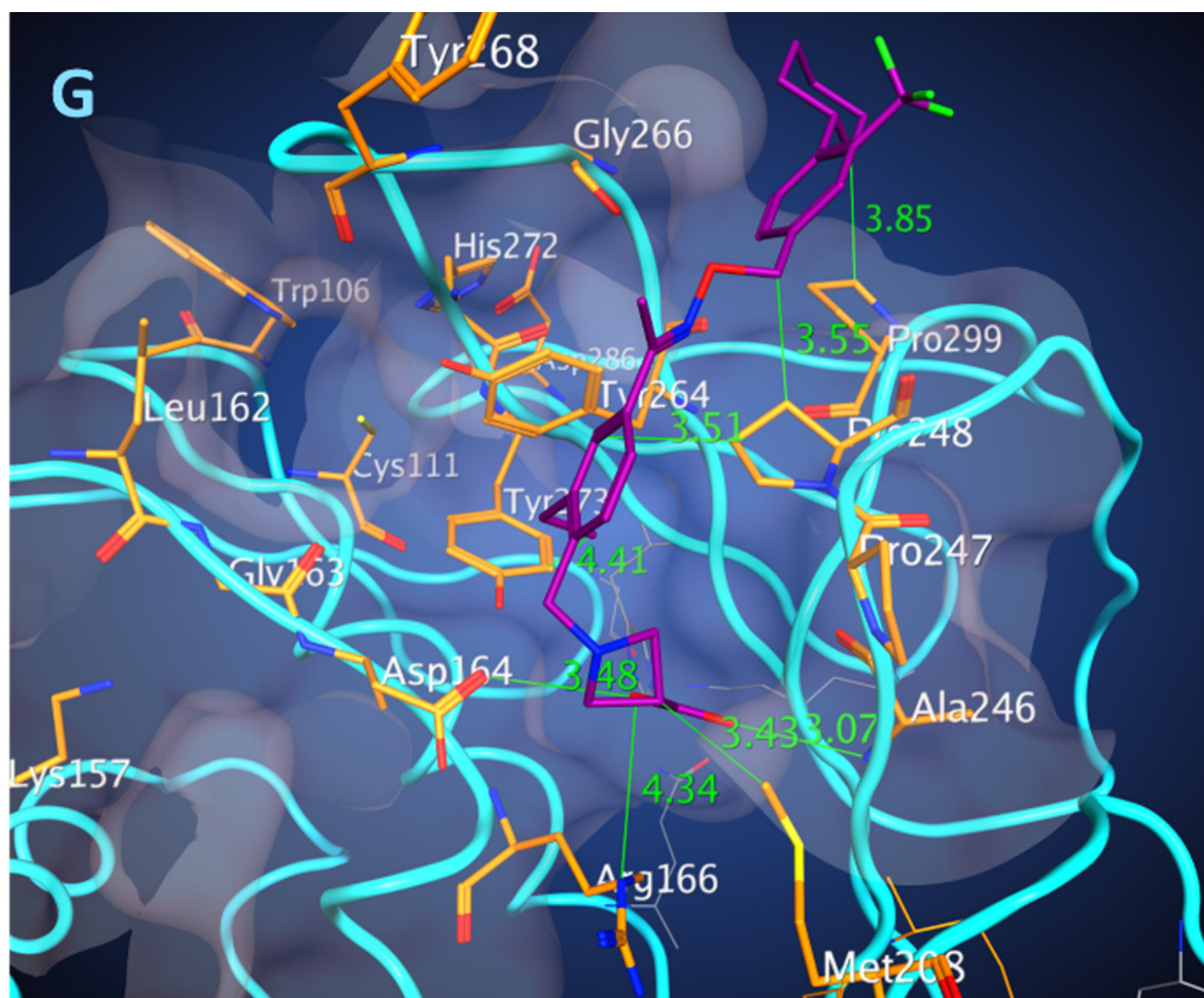
Figure 8

Binding position of the drugs with the best scores in papain-like protease.

Sorafenib, (DFE) = −8.0 kcal/mol.
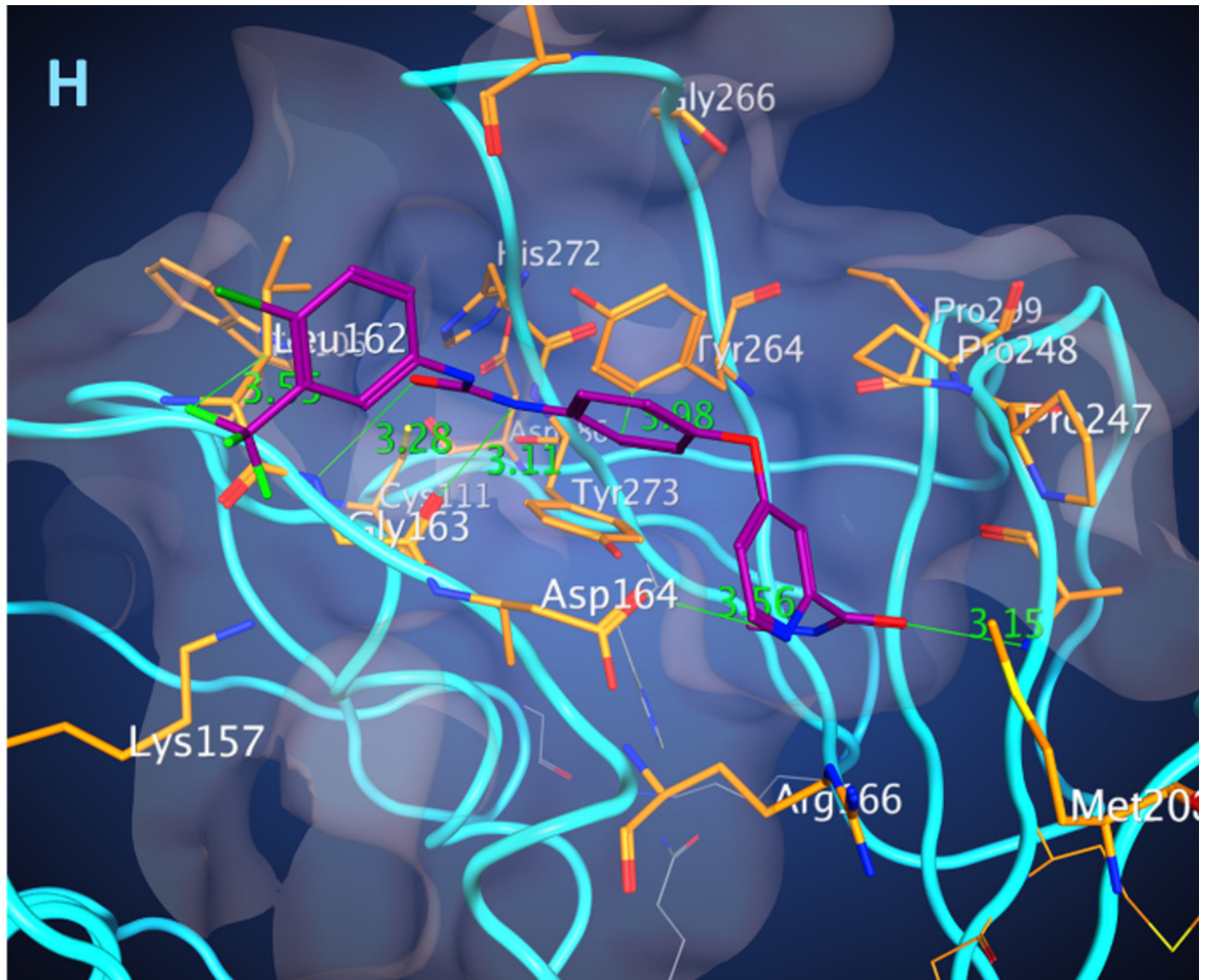
Figure 9

Flexible alignments of compounds in clusters selected by the pharmacophore-based search of possible drug-candidates in the conformational database of FDA-approved drugs having the best docking energies.

Cluster B (20 compounds)
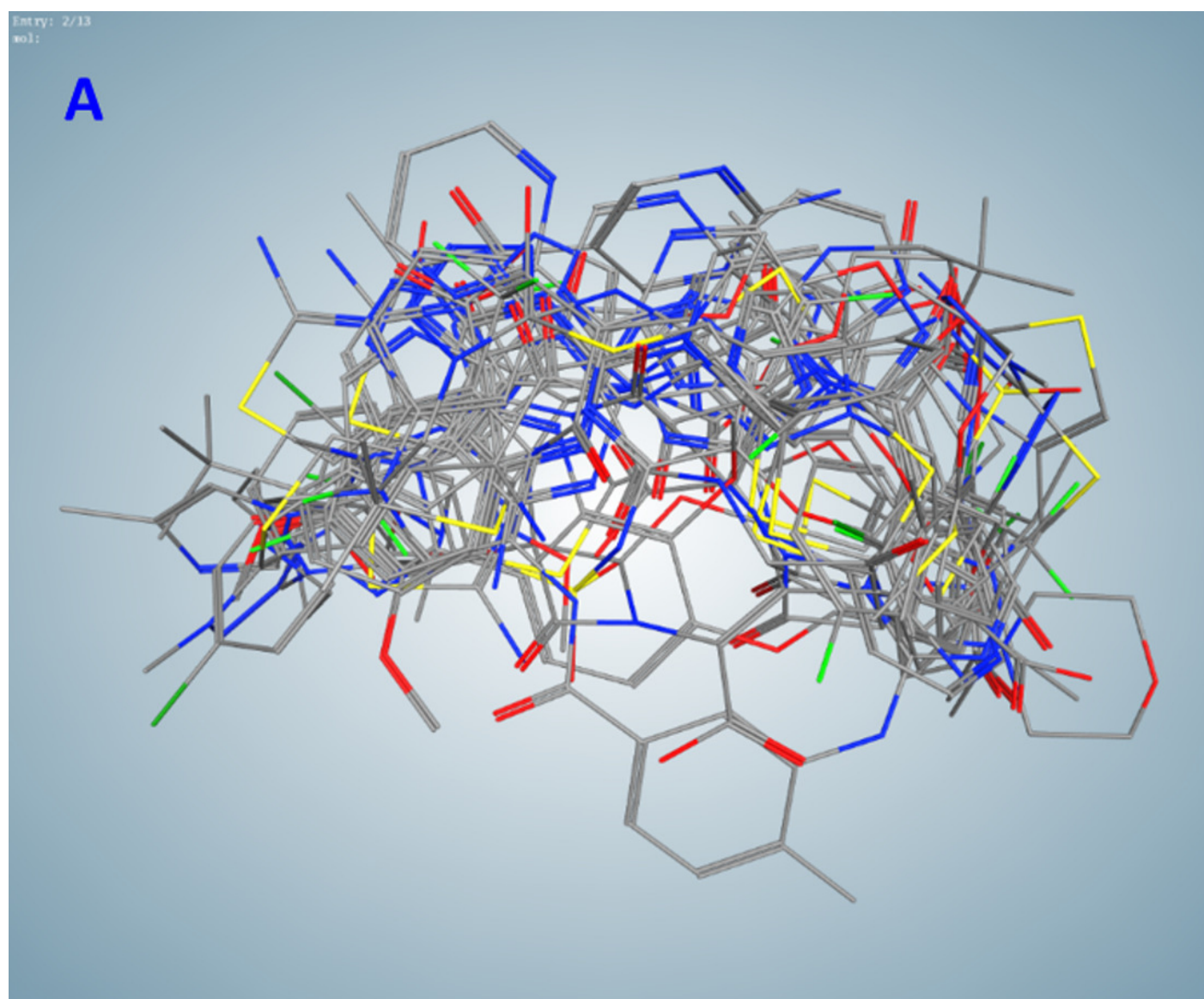
Figure 10

Flexible alignments of compounds in clusters selected by the pharmacophore-based search of possible drug-candidates in the conformational database of FDA-approved drugs having the best docking energies.

Cluster C (9 compounds).
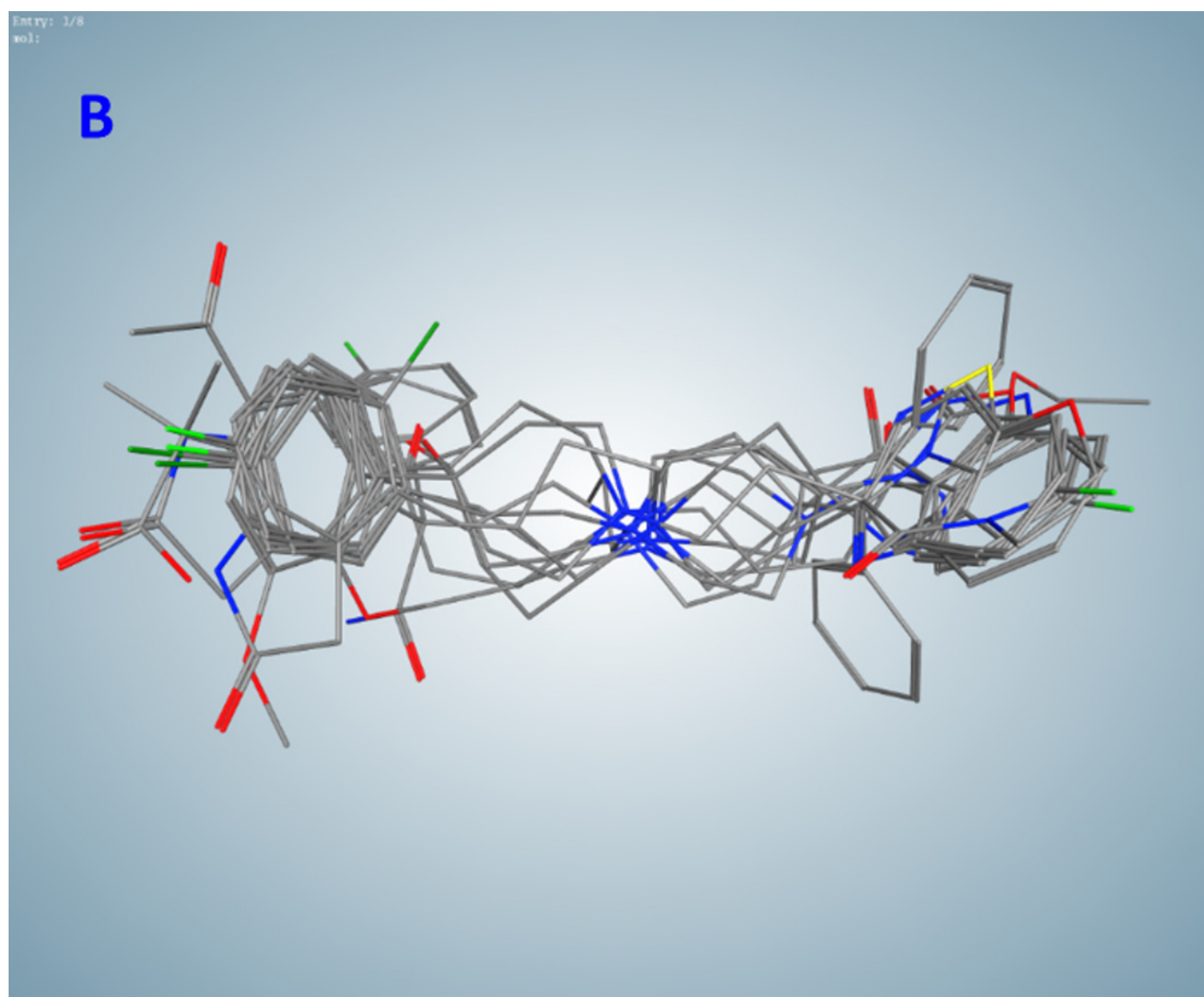
Figure 11

Free energies of docking interactions of selected and random compounds with PL^{pro}.

Minimal energies of the selected and random compounds are −9.3 and −7.7 kcal/mol respectively.
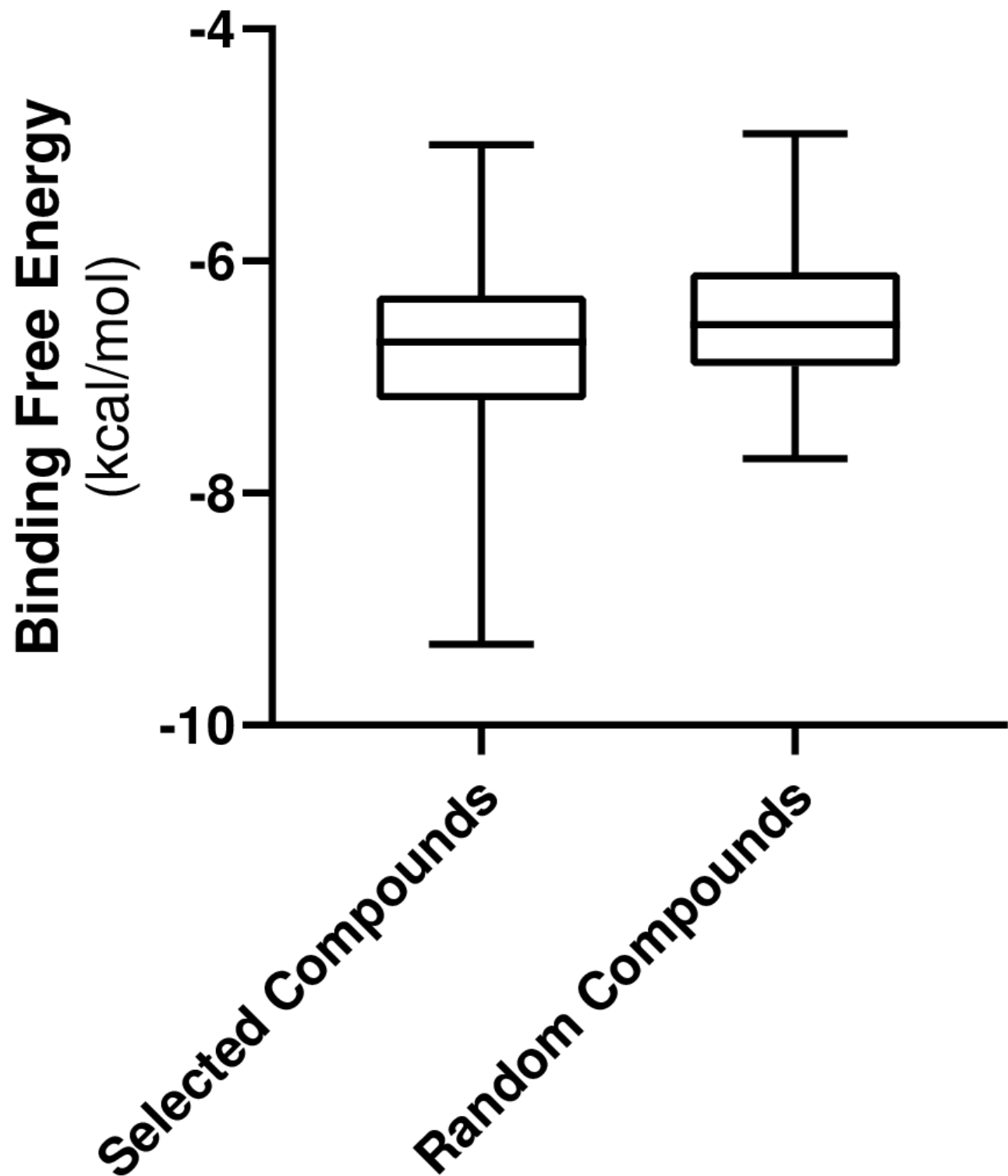
Figure 12

Drugs among the predicted by pharmacophore search inhibitors of PL^pro that were experimentally tested for various viruses
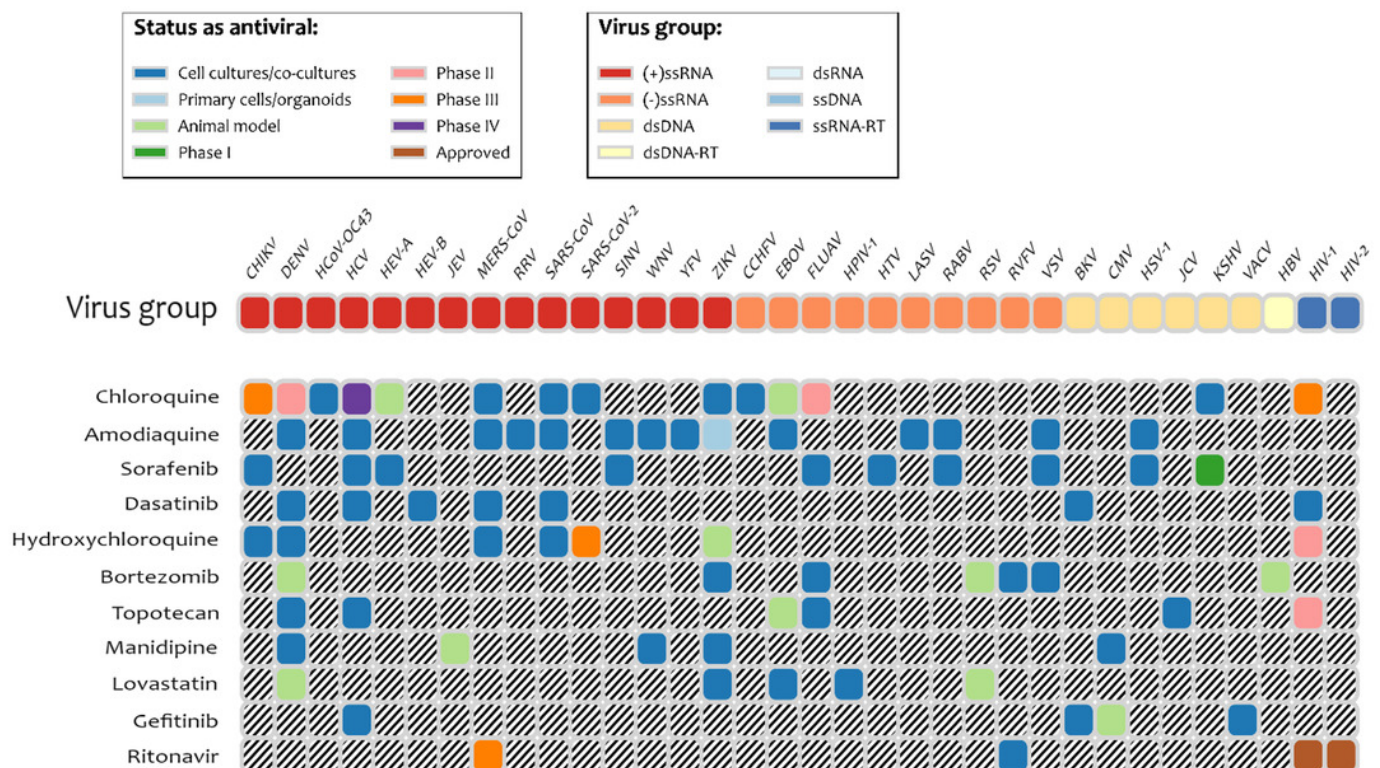
Obtained using DrugVirus.info database [26]

Drug-candidates clustered by fingerprint similarity–overlap alignment.

1 **Table 1.** Drug-candidates clustered by fingerprint similarity–overlap alignment.

Cluster						
A	**B**	**C**	**D**	**E**	**F**	**G**
Alclometasone alpha-Tocopherol acetate	Abemaciclib	Bilastine	Dipyridamole	Acebutolol	Isoetharine	Lactulose
Bimatoprost	Bosentan	Darifenacin	Enoxacin	Atenolol	Isoxsuprine	Micronomicin
Boceprevir	Cefdinir	Droperidol	Gatifloxacin	Betaxolol	Nylidrin	Netilmicin
Buprenorphine	Cefmenoxime	Fluspirilene	Gemifloxacin	Bisoprolol	Protokylol	Tobramycin
Calcitriol	Cefmetazole	Haloperidol	Moxifloxacin	Celiprolol		
Diflorasone	Cefotaxime	Iloperidone		Esmolol		
Dihydroergocryptine	Cefotiam	Loperamide		Metipranolol		
Flunisolide	Cephaloglycin	Ropinirole		Metoprolol		
Fluocinolone acetonide	Copanlisib	Ziprasidone		Nadolol		
Ibutilide	Dasatinib			Propafenone		
Iloprost	Dicloxacillin					
Lapyrium	Doxazosin					
Lovastatin Methyl undecenoyl leucinate	Enasidenib					
Retapamulin	Flucloxacillin					
Ritonavir	Gefitinib					
Travoprost	Latamoxef					
Vitamin E Succinate	Nilotinib					
Zucapsaicin	Prazosin					
	Riociguat					
	Vemurafenib					

List of docked compounds sorted by their energies of interaction with COVID-19 papain-like protease in the docked positions

1   **Table 2.** List of docked compounds sorted by their energies of interaction with COVID-19
2   papain-like protease in the docked positions

Drug name	DFE* energy	Cluster	Drug name	DFE* energy	Cluster
Nilotinib	-9.3	B	Losartan	-7.3	aa
Irinotecan	-8.5	S	Tolvaptan	-7.3	S
Levomefolic acid	-8.4	S	Darifenacin	-7.3	C
Enasidenib	-8.1	B	Flunisolide	-7.3	A
Siponimod	-8.0	S	Alvimopan	-7.2	hh
Sorafenib	-8.0	S	Iloperidone	-7.2	C
Dihydroergocryptine	-8.0	A	Indacaterol	-7.2	S
Abemaciclib	-7.9	B	Mirabegron	-7.2	S
Ziprasidone	-7.9	C	Ximelagatran	-7.2	S
Pemetrexed	-7.8	hh	Droperidol	-7.2	C
Doxazosin	-7.8	B	Ertapenem	-7.2	jj
Axitinib	-7.7	S	Ivacaftor	-7.1	S
Indinavir	-7.7	S	Loperamide	-7.1	C
Lymecycline	-7.7	S	Flibanserin	-7.1	S
Methysergide	-7.7	I	Brexpiprazole	-7.0	C
Rutin	-7.7	S	Cefmenoxime	-7.0	B
Vemurafenib	-7.7	B	Latamoxef	-7.0	B
Glyburide	-7.7	dd	Olmesartan	-7.0	aa
Trabectedin	-7.6	S	Bilastine	-6.9	C
Dasatinib	-7.6	B	Bosentan	-6.9	C
Methylergonovine	-7.5	I	Cefdinir	-6.9	C
Riociguat	-7.5	B	Cefotaxime	-6.9	B
Fluocinolone	-7.5	A	Prazosin	-6.9	B
Fluspirilene	-7.5	C	Retapamulin	-6.9	A
Isavuconazole	-7.4	S	Ritonavir	-6.9	A
Manidipine	-7.4	ii	Sulfasalazine	-6.9	S
Regadenoson	-7.4	S	Topotecan	-6.9	H
Glimepiride	-7.4	dd	Copanlisib	-6.9	B
Canagliflozin	-7.3	bb	Diflorasone	-6.9	A
			Gemifloxacin	-6.9	H

3   *Docking free energy; S- single compound cluster